Surface Texturization of Breast Implants Impacts Extracellular Matrix and Inflammatory Gene Expression in Asymptomatic Capsules

Isabelle I. Brigaud, Charles Garabedian, Nathalie Bricout, Laurent Pieuchot, Arnaud Ponche, Raphaël Deltombe, Rémi Delille, Michael Atlan, Maxence Bigerelle, Karine Anselme

Surface texturation of breast implant impacts extracellular matrix and inflammatory gene expression in asymptomatic capsule

Isabelle **Brigaud**[1,2](PhD), Charles **Garabédian**[3] (MSc), Nathalie **Bricout**[4] (MD), Laurent **Pieuchot**[1,2] (PhD), Arnaud **Ponche**[1,2] (PhD), Raphaël **Deltombe**[3] (PhD), Rémi **Delille**[3] (PhD), Michael **Atlan**[5,6] (MD, PhD), Maxence **Bigerelle**[3] (PhD), Karine **Anselme**[1,2] (PhD)

1. Université de Haute-Alsace, CNRS, IS2M UMR 7361, F-68100 Mulhouse, France

2. Université de Strasbourg, France

3. Université de Valenciennes et du Hainaut-Cambrésis, LAMIH UMR CNRS 8201, Valenciennes, France

4. Private Hospital Saint Germain, Saint-Germain-en-Laye, France

5. Plastic Reconstructive Surgery, Microsurgery, Tissular Regeneration Department, Tenon Hospital Paris, F-75020 Paris, France.

6. Université de Médecine de la Sorbonne, Paris VI, F-75013 Paris, France.

Corresponding authors:

Brigaud Isabelle, PhD

Institut de Science des Materiaux de Mulhouse

IS2M - UMR CNRS 7361 - UHA

15 rue Jean Starcky, B.P. 2488

68057 Mulhouse Cedex, France

isabelle.brigaud@uha.fr

Karine Anselme, PhD

Institut de Science des Materiaux de Mulhouse

IS2M - UMR CNRS 7361 - UHA

15 rue Jean Starcky, B.P. 2488

68057 Mulhouse Cedex, France

karine.anselme@uha.fr

Financial disclosure statement: the authors have the following to disclose

Dr Bricout is an R&D consultant for Groupe Sebbin. Mr Garabédian is employed by Groupe Sebbin. His PhD research is funded by Sebbin, as part of the French government CIFRE program (grant CIFRE 2015– 0843). The other authors declare no potential conflicts of interest with respect to the research, authorship, and publication of this article.

Presented at:

1) **IMCAS**, Paris, France, 31th January-2nd February 2019. “Surface texturation of breast implant impacts extracellular matrix and inflammatory gene expression in asymptomatic capsule” (oral). I Brigaud, C Garabédian, N Bricout, K Anselme

2) MATERIAUX, Strasbourg, France, November 19-21th 2018; “New, simple and biologically validated breast implant classification” (poster). C. Garabédian, I. Brigaud, L. Pieuchot, A. Ponche, M. Bigerelle, K. Anselme

3) ESB, Maastricht, Holland, September 9-13 2018. Molecular biology-based breast implant surface classification (poster). C. Garabédian, I. Brigaud, K. Anselme, M. Bigerelle

4) BIOMAT, Ambleteuse, France, June 12-16 2017. Biomarker-based evidence of the breast implant texturation benefit (oral). C. Garabedian, I. Brigaud, M. Bigerelle, K. Anselme

Short Running Head: Breast implant surface texturing effects

ABSTRACT

Background: Texturing processes have been designed to improve biocompatibility and mechanical anchoring of breast implants. However, high texturing degree has been associated with severe pathologies. Here, we aimed to determine whether implant surface topography could also affect physiology of asymptomatic capsules.

Methods: We collected topographical measurements from 17 different breast implant devices by interferometry and X-ray microtomography. Morphological structures were statistically analyzed to obtain a robust breast implant surface classification. We obtained 3 topographical categories of textured implants ("peak and valleys", "open cavities", and "semi-opened cavities") based on the cross-sectional aspects. We simultaneously collected 31 Baker I capsules, sorted them according to the new classification, established their molecular profile, and examined the tissue organization.

Results: Each of the categories showed distinct expression patterns of genes associated with the extracellular matrix (*Timp* and *Mmp* members) and inflammatory response (*Saa1*, *Tnsf11*, *Il8*), despite originating from healthy capsules. Besides, slight variations were observed in the organization of capsular tissues at the histological level.

Conclusions: We combined a novel surface implant classification system and gene profiling analysis to show that implant surface topography is a bioactive cue that can trigger gene expression changes in surrounding tissue, even in Baker I capsules. Our new classification system avoids confusions around the word "texture", and could be transposed to implant ranges of every manufacturer. This new classification could prove useful in studies on potential links between specific texturations and the incidence of certain breast-implant associated complications.

INTRODUCTION

Breast implant design involves the selection and combination of several features such as implant filling (silicone gel or saline solution), shape (round or anatomically shaped), volume, and surface (smooth or textured). Implant surface is essential to the performance and safety of breast implant devices. Surface topography—the intricate relief of the outer implant shell—directly affects soft tissue reaction and fibrous tissue formation around the implant, which, if disrupted, could lead to post-surgery complications such as capsular contracture.[1,2] The link between texturation of implant surface and medical outcomes remains controversial. "Macrotextures" were designed to promote tissue adhesion to the implant.[3] However, their impact on capsular contracture[4–7] and rare long-term complications such as double capsule[8], late seroma, and breast implant-associated anaplastic large cell lymphoma (BIA-ALCL)[9–13] remains unclear. The relationship between the mechanisms governing breast implant biocompatibility associated with implant surface properties is therefore of great interest.

The formation of capsular tissue around an implant is a physiological wound-healing response to foreign elements. The host organism reacts to the presence of an implant by eliciting local extracellular matrix (ECM) reorganization. These events are tightly regulated by the TGFβ signaling pathway, which directly mediates downstream expression of about 60 ECM-related genes, including the expression balance of matrix-remodeling enzymes such as metalloproteinases (*MMPs*) or tissue inhibitors of proteinases (*TIMPs*).[14] The inflammatory response plays a major role in implant integration[15], which can also be promoted by MMPs.[16] Capsule formation typically isolates the foreign body from the host tissue, after which the reaction becomes quiescent or ceases, resulting in a stable, compatible, and soft peri-prosthetic capsule. We hypothesized that breast implant topography could mediate cell signaling, particularly during the initial formation of capsular tissue. We assumed that different degrees

of surface texturation would elicit specific gene activation/response profiles in peri-prosthetic cells, even in healthy tissues such as Baker I capsules.[17]

In this study, we conducted a statistically robust but simple and comprehensive classification of breast implants based on the degree of surface texturation. We then compared the impact of different categories of implants on the expression of a panel of ECM and inflammatory genes in healthy capsules. We also examined the effect of such implants on peri-prosthetic tissue organization.

MATERIALS AND METHODS

Substrate surface measurement

Surface topography of 17 implant types from 11 independent companies were measured and analyzed as a representative sample of available marketed implants (see table, supplemental digital content 1). The devices examined were new, sterile, and within their period of use. We collected 3 sets of samples from 3 separate locations (dome, edge, and base), obtaining 9 independent measures per implant. Each sample was taken from the implant shells by using a punch to obtain a final circular area of 10 mm², and sonicated in 10% alcohol solution for 10 minutes for cleaning. Samples were measured by interferometry (NewView™ 7300 Optical Surface Profiler; Zygo Corp., Middlefield, CT, USA) for “peak and valley” (PV)-patterned surfaces or X-ray Microtomography (SkyScan™ 1172; Bruker BioSpin Corporation, Billerica, MA, USA) for “open-cavities (OC)” and “semi-opened cavity" (SOC)-patterned surfaces, as described previously.[18] Based on the international breast implant standard (ISO 14607:2018), we restricted our measurements to 4mm^2 within the circular sample.

Implant type	Company
Biocell™ Microcell™	Allergan (Dublin, Ireland)
Round microtextured implant Round textured implant Shaped textured implant Round smooth implant	Sebbin (Boissy, l'Aillerie, France)
Cereform®	Cereplas (Sailly lez Cambrai, France)
Siltex®	Mentor (Irvine, CA, USA)
TRUE Texture®	Sientra (Santa Barbara, CA, USA)
Cristalline Micro-textured Cristalline Textured	Eurosilicone (Apt, France)
POLYtxt® MESMO® sensitive	Polytech Health and Aesthetics (Dieburg, Germany)
SilkSurface™	Motiva/Establishment Labs (Alajuela, Costa Rica)
Nagotex®	Nagor (Glasgow, UK)
Perthese®	Perouse Plastie (Bornel, France)
Round microtextured implant Shaped textured implant	Arion (Mougins Sophia-Antipolis, France)

supplemental digital content 1. Breast implant sampling used to establish topography-based classification. Commercial designation and company for each sample are specified.

Classification

Topography-based breast implant classification was established using robust statistical discriminant analyses, which will be described in detail in a subsequent publication. Briefly, surface topography measurements were computed using Mountains® software (Digital Surf, Besançon, France) and MesRug® (MesRug Data System, Lieu Saint Amand, France). By applying filters, surfaces were decomposed in elementary surfaces to scale down intricate surface roughness properties. This process was applied independently to the 42 most common roughness parameters (defined in ISO 25178 and EUR 15178N). Classification was established based on the resulting values. Implants were categorized according to morphological features observed from surface cross-section and topography analyses as "peak and valley" (PV), "open-cavities (OC)", and "semi-opened cavity" (SOC). Cross-sections based on samples analyzed by

X-ray microtomography were established after image reconstruction as described previously.[18] For the interferometric measurements, a 2mm-long profile was extracted from the topography, by using the Mountains® software, to construct the cross-section.

Patient information and related breast implant capsule sampling

Twenty female patients with 7 different types of textured breast implants, who underwent breast revision surgeries between February 2017 and February 2018, were recruited for this study (average age: 51 ± 15 years). A single surgeon performed all surgeries and tissue collection. Ethical approval was obtained from the institutional review board. Patients gave informed consent prior to participating. Thirty-one capsular tissue samples were collected; 5 were harvested from reconstructed breasts, and the rest from aesthetic surgeries. Fig.1 shows the reasons for revision surgery.

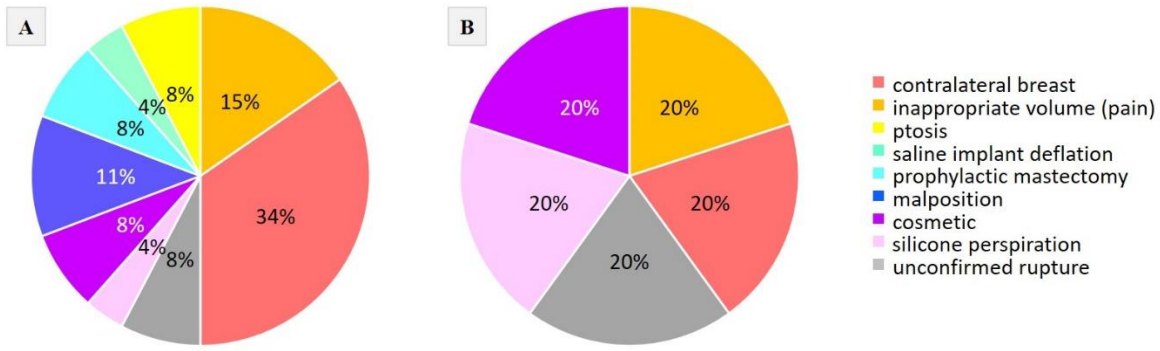

Figure 1. Recapitulative diagrams of the clinical reasons for implant removal. Percentage (%) of collected capsules A) after aesthetic surgery (n = 26) and B) after breast reconstruction (n = 5).

The mean duration of implantation was 9 ± 6 years (range: 1–21 years). Implant location was subglandular for 11 implants and submuscular for 16. Two devices were implanted under a flap while the positions of 2 implants were not reported. Twenty-eight implants were silicone gel-filled and 3 were saline-filled. The mean implant volume was 286 ± 96 ml (range: 120-525 ml). For more clarity, data are summarized in Fig. 2. In this study, we restricted our sampling to Baker I-classified capsular tissues.[17] Samples from patients carrying gene mutations for fibrosis or with assessed implant rupture were excluded.

reference to classification	**substrate types of the harvested tissues**	**capsules**		**age or mean age of the patients (years)**	**implant position**			
		total sampling = 31 capsules including 20 patients	duration or mean duration of implantation (years)		SG	SM	FLAP	NR
peaks and valleys (PV)	round microtextured implant (Sebbin)	2 (including 1 patient)	1	25	-	2	-	-
	Cereform® (Ceraplas)	5 (including 3 patients)	7.2 (from 4 to 9)	43.6 (from 34 to 47)	5	-	-	-
open cavities (OC)	Siltex® (Mentor)	1 (including 1 patient)	18	43	-	1	-	-
	round textured implant (Sebbin)	9 (including 6 patients)	10.3 (from 1 to 15)	54.8 (from 20 to 79)	5	4	-	-
	TRUE Texture® (Sientra)	2 (including 1 patient)	21	58	-	2	-	-
semi-opened cavities (SOC)	shaped textured implant (Sebbin)	8 (including 6 patients)	7.8 (from 5 to 10)	58.1 (from 46 to 71)	1	5	2	-
	Biocell™ (Allergan)	4 (including 2 patients)	5 (from 2 to 8)	47 (from 46 to 48)	-	2	-	2

Figure 2. Recapitulative tab gathering implant characteristics and patient clinical data established from the periprosthetic breast capsule (Baker I) tissue sampling. Implant positions: subglandular (SG), submuscular (SM), not reported (NR).

RNA extraction, cDNA synthesis, and quantitative PCR

Collected tissues were immediately stored in RNA later solution (Invitrogen™) at -20°C until further use. For RNA extraction, tissues were sequentially chopped into small pieces with a razor, placed in an Eppendorf containing 600 µL of chilled Trizol, crushed manually, and vortexed for 5 min at max speed (3200 rpm). Total RNA was extracted using the Direct-zol™ RNA MiniPrep (Ozyme), according to the manufacturer's instructions. RNA purity and concentration were evaluated using a NanoDrop One^{C} (Thermo Fischer Scientific). cDNAs were synthesized from samples normalized to 500 ng RNA, by using the iScript™ cDNA synthesis Kit (Bio-Rad). qPCR was carried out as described previously.[19] Calibration sample was facing an OC-patterned topography and served to calculate relative gene quantifications for all the samples, irrespectively of texture group.

Histological studies

Histological studies were performed on peri-prosthetic capsules surrounding only OC- and SOC-patterned implants and samples were collected from the same specimens used for

molecular experiments. Medical protocol did not allow histological studies on patients undergoing surgery for aesthetic reasons, which included all 8 PV-patterned implants. Serial sections of 3-µm thickness were cut from paraffin-embedded breast capsules by using a microtome, and subsequently stained using hematoxylin-eosin. Images were acquired using light microscopy under ×20 objective (Nikon Eclipse Ts2). Features that were analyzed included presence of immune cells, vascularization, structures of collagen matrix, and absence of malignancy.

qPCR statistical analyses

Molecular gene expression profiles were generated as boxplots with mean value, standard error of the mean (SEM), and outliers, by using the Plotly software. Statistical analyses were performed by using Student *t*-test and non-parametric Mann-Whitney post-test (GraphPad Prism Software, San Diego, CA, USA). From these analyses, the level of significance was considered to be $p < 0.001$. Because of intrinsic constraints linked to the qPCR technique, we considered samples as *biologically* different for expression ratios higher (overexpression) or lower (repression) than ×3, even if statistical tests were positive.

RESULTS

CLASSIFICATION

Fig. 3 illustrates topographical features shared by implants grouped in the same category, giving a representative aspect of the outer implant shell which directly contacts breast tissues. PV-patterned surfaces displayed regular peak and valley structures with heights of low amplitude (<100 µm). In comparison, OC-patterned surfaces mostly presented curve-shaped open cavities features of amplitude ranging from 50 µm to 300 µm. Topographies and cross-sections of SOC-surfaces showed repetitive and regularly distributed unsealed cuboid-like patterns of high amplitude (>400 µm). Cuboid structures protruding from the main surface exposed thin and

angled edges at the implant interface. This specific cuboid pattern is generated by salt-loss technique followed by surface brushing treatment.

classes	prostheses sampling	topographies	cross-sections
peak and valley-patterned surfaces (PV)	▪ SilkSurface™ (Motiva) ▪ Round microtextured implant (Arion) ▪ Perthese® (Perouse) ▪ Cereform® (Cereplas) ▪ Round microtextured implants (Sebbin)	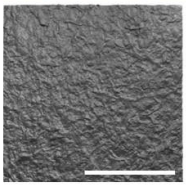	
open cavity-patterned surfaces (OC)	▪ Round textured implant (Sebbin) ▪ TRUETexture® (Silimed) ▪ MESMO® sensitive (Polytech) ▪ Nagotex® (Nagor) ▪ Microcell™ (Allergan) ▪ Cristalline Micro-textured (Eurosilicone) ▪ POLYtxt® (Polytech) ▪ Siltex® (Mentor)	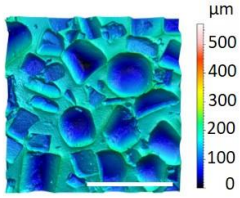	
semi-opened cavity-patterned surfaces (SOC)	▪ Cristalline Textured (Eurosilicone) ▪ Shaped textured implant (Sebbin) ▪ Shaped textured implant (Arion) ▪ Biocell™ (Allergan)	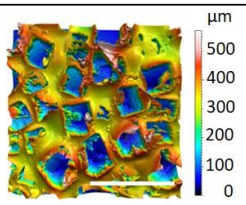	

Figure 3. illustration of the main surface structures shared by breast implant devices binding in each of the 3 categories, namely PV, OC and SOC. Top view topography and corresponding cross-section is given for one device (underlined market reference) as a representative example of the entire category. A color calibration bar in micrometer (µm) indicates the height of the relief on the topographies where black and red represents respectively the lowest and the highest amplitude of topography. Bar scale represents 1,0 mm in length.

GENE EXPRESSION

We evaluated the effects of the 3 breast implant topographical classes in healthy samples on expression of foreign body reaction and inflammatory related genes, and capsular tissue organization. We excluded any chance of expression of the BIA-ALCL markers *Cd30* and *Alk* in our sampling.[20] These two markers were not significantly present in our entire sample set (data not shown).

Relative expression of matrix metalloproteinases (MMPs)

Figure 4 shows the relative expression of *Mmp2*, *MMp9,* and *Mmp12*. No significant change in *Mmp2*, *Mmp9,* or *Mmp12* expression levels were observed in peri-prosthetic cells in contact

with PV-patterned surfaces compared to the OC group. On the contrary, *Mmp2* levels were unchanged (Fig. 4A), and *Mmp9* and *Mmp12* were significantly up-regulated (44 ± 11 and 46 ± 21-fold respectively) in tissues in contact with SOC-patterned implants, compared to those in contact with PV- and OC-patterned implants (Fig. 4B and 4C). Thus, SOC-patterned implants likely trigger *Mmp9* and *Mmp12*, but not *Mmp2*, in the surrounding tissues.

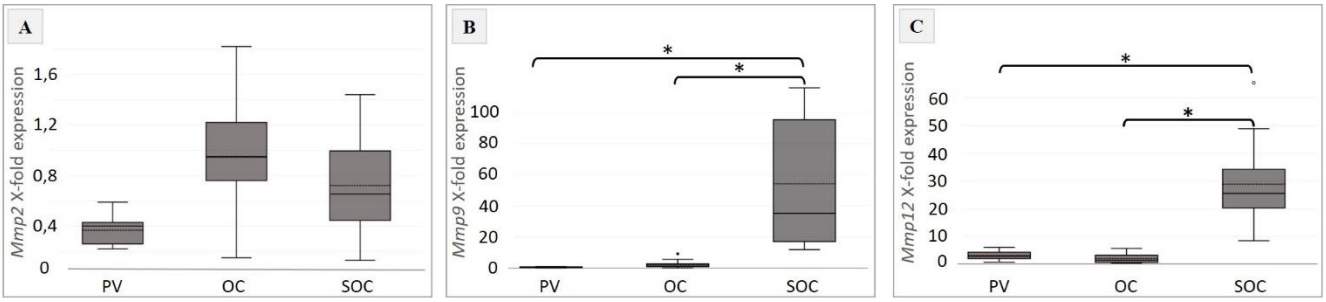

Figure 4. Boxplots depicting relative gene expression levels Mmp2 (A), Mmp9 (B), and Mmp12 (C) in healthy tissue (Baker I grade) in contact with peak and valley (PV), open cavities (OC), or semi-opened cavity (SOC)-patterned breast implants. Empty circles correspond to outlier values, dotted and full lines correspond to the mean and median values respectively. * $p < 0.001$ (Student t-test and non-parametric Mann Whitney tests).

Relative expression of tissue inhibitor of metalloproteinases (TIMPs)

Because TIMP activity closely balances that of the MMPs, we focused our analyses on this gene category (Fig. 5). In tissues in contact with PV-patterned implants, we found that *Timp4* gene expression was significantly up-regulated (4.48 ± 0.94-fold; Fig. 5C) compared to that in tissues associated with OC (1.42 ± 0.20-fold) or SOC (0.35 ± 0.04-fold) patterned implants. In tissues in contact with SOC-patterned implants, *Timp1* and *Timp4* gene expression varied inversely, with *Timp1* expression significantly up-regulated (4.0 ± 0.61-fold; Fig. 5A) and *Timp4* expression down-regulated (0.35 ± 0.04-fold) compared to the PV and OC groups (Fig. 5C). *Timp2* gene expression was not significantly different in the three groups (Fig. 5B). We concluded that contact of PV and SOC-patterned implants with peri-prosthetic tissues affects *Timp1* and/or *Timp4* expression.

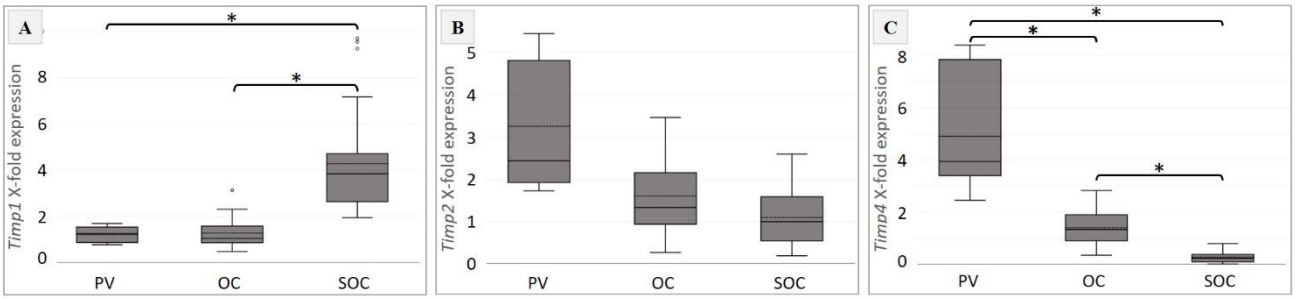

Figure 5. Boxplots depicting relative gene expression levels of tissue inhibitors of metalloproteinases Timp1 (A), Timp2 (B), and Timp4 (C) from healthy tissue (Baker I grade) in contact with peak and valley (PV), open cavities (OC), or semi-opened cavity (SOC)-patterned breast implants. Empty circles correspond to outlier values, dotted and full lines correspond to the mean and median values respectively. * $p < 0.001$ (Student t-test and non-parametric Mann Whitney test).

Relative expression of genes related to the inflammatory response

Immunological response mechanisms are essential for implant integration. We therefore examined the expression of different genes involved in these processes (Figure 6). Variations in *Tgfβ1* (Figure 6A) and *Saa1* (Figure 6B) expression were not significant among the samples tested. Capsular tissues located in the vicinity of SOC-patterned implants exhibited up-regulated expression of *Il8* (3.95 ± 0.96-fold) compared to those in the OC and PV-patterned implant groups (Figure 6C). *Tnfs11* was drastically down-regulated in the SOC-patterned implant group (0.19 ± 0.04-fold) compared to the OC (1.15 ± 0.20-fold) and PV (0.88 ± 0.09-fold) groups. Thus, peri-prosthetic cells elicit immunological responses, when in contact with an implant surface, which depend on the topography of the implant.

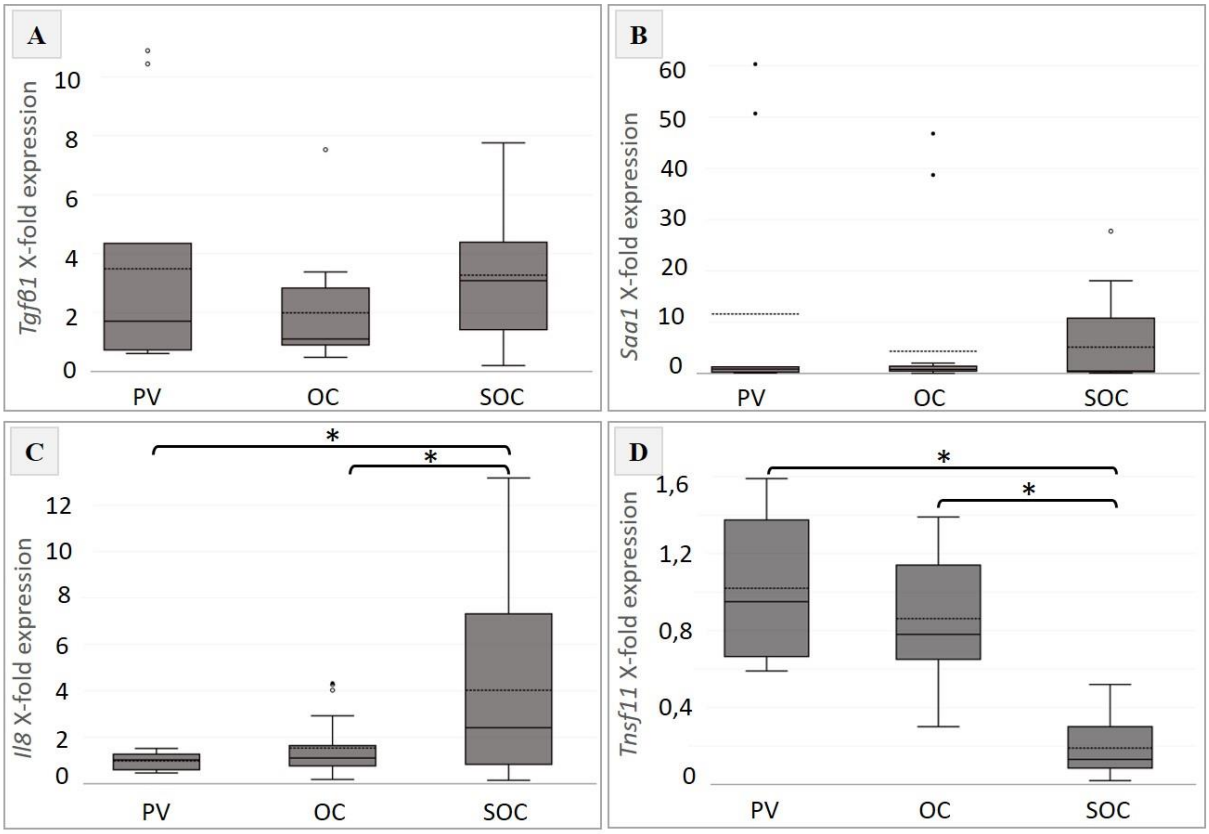

Figure 6. Boxplots depicting relative gene expression levels of the pro-fibrotic transforming growth factor beta 1 Tgfβ1 (A), TNF superfamily member11 (Tnfs11) (B), C-X-C motif chemokine ligand 8 (Il8) (C), and inflammatory markers serum amyloid 1 (Saa1) (D) from healthy tissue (Baker I grade) in contact with peak and valley (PV), open cavities (OC), or semi-opened cavity (SOC)-patterned breast implants. Empty circles correspond to outlier values, dotted and full lines correspond to the mean and median values respectively. * $p < 0.001$ (Student t-test and non-parametric Mann Whitney tests).

HISTOLOGICAL ANALYSES

Histology of capsules located near OC- or SOC-patterned implants revealed discrete differences in tissue organization. Irrespective of the nature of the implant, we observed tissues with tightly woven fibroblast fibers oriented parallel to the implant surface. A layer of immune mononucleated cells of variable density was observed directly at the implant interface, and their distribution was more scattered within the capsules. Compared to tissues facing OC-patterned surfaces, tissues facing SOC-patterned surfaces exhibited more fibro-hyaline structures and a higher occurrence of small congestive capillary vessels (Figure 7). We concluded that SOC-patterned implants promote discrete tissue vascularization.

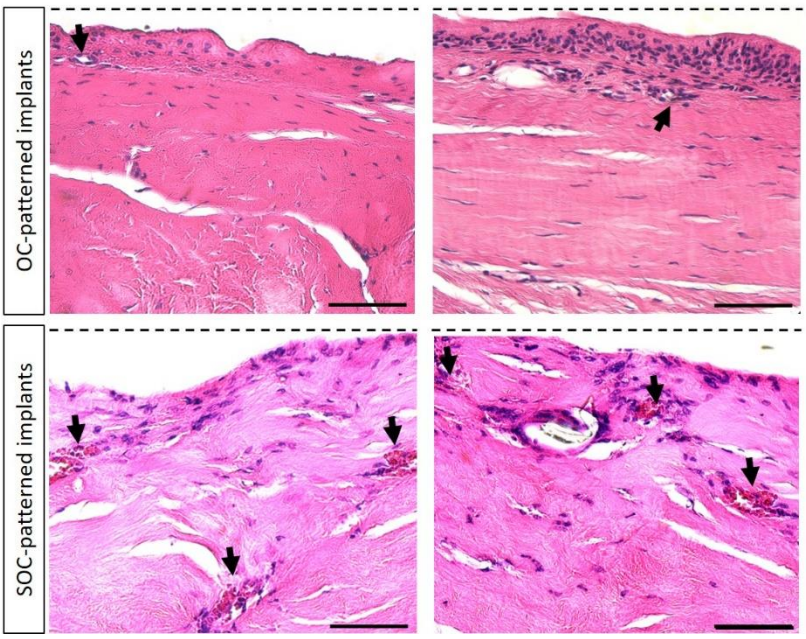

Figure 7. Histological characteristics of Baker I breast tissues in contact with OC-patterned implants or SOC-patterned implants. Images from 2 independent patients for each condition. No malignancies were identified. Tissues facing OC- or SOC- patterned implants exhibit tightly woven fibroblast fibers oriented parallel to the implant surface. Irrespective of the implant texturation, tissues commonly exhibited a layer of mononucleated cells at the implant interface (dotted line) together with discrete and scattered distribution of histiocytes within the inner part of the capsules. Compared to tissues facing OC-patterned surfaces, tissues facing SOC-patterned surfaces exhibited more fibro-hyaline structures together with small congestive capillary vessels (black arrows). Scale bar: 100 µm.

DISCUSSION

Elucidating the relationship between degree of breast implant surface texturation and clinical outcomes could greatly improve implant integration. In this study, we linked for the first time characteristics of implant surface topography to gene response in host healthy tissues. We used a new breast implant classification system based on robust statistical analyses, with simple and meaningful nomenclature. Detailed comparison with existing classifications ([21,22,23]), although important, are beyond the scope of this report and will be discussed in a subsequent paper. Briefly, our new classification provides a relevant tool to standardize breast implant prostheses into topographical categories with the aim to end with confusions existing around the employment of the word “texture”. In light of our new classification, we examined the expression profiles of genes that are essential to foreign body reaction. The formation of capsular tissue around an implant involves inflammatory and ECM remodeling responses mediated by TGFβ1. *Tgfβ1* expression was found at a basal level, indicating that wound healing was completed and the peri-prosthetic capsule had reached a steady state. Thereafter, we determined whether the establishment of appropriate bio-interfaces between peri-prosthetic cells and dissimilar breast implant topographies was associated with specific reprogramming of

dynamic MMP/TIMP balance activity. ECM-related gene expression levels were significantly affected by the different surfaces. Compared to OC-patterned surfaces, our internal reference for gene variations, only PV-patterned surfaces were correlated with *Timp4* up-regulation, indicating that host organisms recognize these two types of surfaces as relatively similar.

The gene expression profile of peri-prosthetic cells in contact with SOC-patterned surfaces was drastically different. *Timp4* and *Tnsfs11* expression was down regulated. Further, *Mmp9, Mmp12, Timp1*, and *Il8* were considerably up regulated. We concluded that establishment of an adequate bio-interface for breast implant integration requires adaptation of peri-prosthetic cells to implant topography, which is molecularly modulated through differential and specific *Mmp*/*Timp* gene expression. Two studies [24,25] have shown that Baker III capsules also exhibit significant changes in *Timp1*, *Timp4*, and *Tnfs11* expression. It is striking that these asymptomatic capsules share molecular hallmarks with contracted (fibrotic) capsules. However, accurate comparison of the gene expression profiles observed in this study with those described previously is not possible because previous studies did not distinguish between degrees of implant texturation and used different internal calibrators for qPCR calculations. Therefore, we could not conclude which type of surface favors capsular contracture. To elucidate this point, further experiments comparing expression levels of these markers in the context of texturation degree in contracted capsules, using our internal calibrator, are required.

At the tissue level, capsules interfacing SOC-patterned implants were associated with slightly higher occurrence of capillary vessels than were OC-patterned implants. Interestingly, *Mmp9* gene expression, which is increased in these capsules, dominates the regulation of angiogenesis through several catalytic and non-catalytic functions. Notably, it releases proangiogenic chemokines such as IL8, whose gene expression was also up-regulated.[26–28] IL8, originally identified as a neutrophil chemoattractant[29], is also known for its pro-inflammatory activity. However, we could not confirm this role, since this type of immune cell was not distinguished

in histological sections. Nevertheless, we observed an accumulation of histiocytes at the interface for any surface, as described in previous studies.[25]

Finally, we observed drastic down-regulation of *Tnsf11*, which is expressed in fibroblasts[30] and is involved in various physiological processes including immunity. TNFSF11 interacts with the immune system via induction of pro-inflammatory cytokines, acting on several immune cells including monocytes, T cells, and B cells. Besides a role in activating the adaptive immune response, it is known to regulate immune tolerance,[31] a process by which the body reduces or eliminates an immune response to chronic agents.[32] Considering its pleiotropic activity, further functional experiments are required to elucidate the role of TNFSF11 in peri-prosthetic cells.

In this study, we showed that at the molecular level, peri-prosthetic cells facing PV or OC-patterned surfaces react similarly, while SOC-patterned surfaces promote drastic gene expression variations. Giot *et al*[8] showed that "macro-texturation" (herein classified in the SOC group) clearly induces strong tissue in-growth into its cavities, which accounts for the exceptional stability of the capsule-implant complex. As illustrated in our implant cross-sections, tissue ingrowth occurs inside unsealed cuboid-like patterns with possibly fragile thin walls. Thus, the shearing forces between implant and capsule caused by natural body movements, applied on strongly attached ingrowth tissue, could induce tissue alterations. The host body is therefore forced to undergo constant tissue remodeling as highlighted by *Mmp/Timp* gene expression modulation.

Our data show that surface topography features give healthy peri-prosthetic cells specific molecular identity, and could, in combination with other factors (such as biofilms), contribute to the development of breast implant-associated complications. Further studies on the combinatorial effects of surface topography with other factors such as presence of a biofilm, degree of capsule adhesion, and implant positioning [6–38] are required. Larger-scale studies both in term of tissue sampling and gene expression analyses (RNAseq) are also required. In

conclusion, design of surface topography is of prime importance to ensure safe and long-term physiological integration of breast implants.

Figure 1. Recapitulative diagrams of the clinical reasons for implant removal. Percentage (%) of collected capsules A) after aesthetic surgery (n = 26) and B) after breast reconstruction (n = 5).

Figure 2. Recapitulative tab gathering implant characteristics and patient clinical data established from the periprosthetic breast capsule (Baker I) tissue sampling. Implant positions: subglandular (SG), submuscular (SM), not reported (NR).

Figure 3. Illustration of the main surface structures shared by breast implant devices binding in each of the 3 categories, namely PV, OC and SOC. Top view topography and corresponding cross-section is given for one device (underlined market reference) as a representative example of the entire category. A color calibration bar in micrometer (µm) indicates the height of the relief on the topographies where black and red represents respectively the lowest and the highest amplitude of topography. Bar scale represents 1,0 mm in length.

Figure 4. Boxplots depicting relative gene expression levels Mmp2 (A), Mmp9 (B), and Mmp12 (C) in healthy tissue (Baker I grade) in contact with peak and valley (PV), open cavities (OC), or semi-opened cavity (SOC)-patterned breast implants. Empty circles correspond to outlier values, dotted and full lines correspond to the mean and median values respectively. * $p < 0.001$ (Student t-test and non-parametric Mann Whitney tests).

Figure 5. Boxplots depicting relative gene expression levels of tissue inhibitors of metalloproteinases Timp1 (A), Timp2 (B), and Timp4 (C) from healthy tissue (Baker I grade) in contact with peak and valley (PV), open cavities (OC), or semi-opened cavity (SOC)-patterned breast implants. Empty circles correspond to outlier values, dotted and full lines correspond to the mean and median values respectively. * $p < 0.001$ (Student t-test and non-parametric Mann Whitney test).

Figure 6. Boxplots depicting relative gene expression levels of the pro-fibrotic transforming growth factor beta 1 Tgfβ1 (A), TNF superfamily member11 (Tnfs11) (B), C-X-C motif chemokine ligand 8 (Il8) (C), and inflammatory markers serum amyloid 1 (Saa1) (D) from healthy tissue (Baker I grade) in contact with peak and valley (PV), open cavities (OC), or semi-opened cavity (SOC)-patterned breast implants. Empty circles correspond to outlier values, dotted and full lines correspond to the mean and median values respectively. * $p < 0.001$ (Student t-test and non-parametric Mann Whitney tests).

Figure 7. Histological characteristics of Baker I breast tissues in contact with OC-patterned implants or SOC-patterned implants. Images from 2 independent patients for each condition. No malignancies were identified. Tissues facing OC- or SOC- patterned implants exhibit tightly woven fibroblast fibers oriented parallel to the implant surface. Irrespective of the implant texturation, tissues commonly exhibited a layer of mononucleated cells at the implant interface (dotted line) together with discrete and scattered distribution of histiocytes within the inner part of the capsules. Compared to tissues facing OC-patterned surfaces, tissues facing SOC-patterned surfaces exhibited more fibro-hyaline structures together with small congestive capillary vessels (black arrows). Scale bar: 100 µm.

Supplemental digital content 1. Breast implant sampling used to establish topography-based classification. Commercial designation and company for each sample are specified.

Acknowledgments We thank Nayana TusamdaWakhloo for feedback on this work and Dr Maria Rosa Katunar (PhD) for help with statistics. We also thank the « NANOTRANSMED » project co-funded by the European Regional Development Fund (ERDF) in the framework of the INTERREG V Upper Rhine program (« Transcending borders with every project ») and by the Swiss Confederation and the Swiss cantons of Aargau, Basel-Landschaft and Basel-Stadt." The topographical measurements were supported by the Project TRIBOSURF and the Platform MORPHOMECA from the ELSAT2020 project, co-financed by the European Union with the European Regional Development Fund, the French state, and the Hauts de France Region Council.

REFERENCES

1. Abramo AC, De Oliveira VR, Ledo-Silva MC, De Oliveira EL. How texture-inducing contraction vectors affect the fibrous capsule shrinkage around breasts implants? *Aesthetic Plast Surg*. 2010;34(5):555-560. doi:10.1007/s00266-010-9495-9.
2. Dolores W, Christian R, Harald N, Hildegunde P, Georg W. Cellular and molecular composition of fibrous capsules formed around silicone breast implants with special focus on local immune reactions. *J Autoimmun*. 2004;23(1):81-91. doi:10.1016/j.jaut.2004.03.005.
3. Wynn T a, Wolfram D, Rabensteiner E, et al. Physico-chemical characteristics of coated silicone textured versus smooth breast implants differentially influence breast-derived fibroblast morphology and behaviour. *Aesthetic Plast Surg*. 2015;34(5):81-91. doi:10.1016/j.jaut.2004.03.005.
4. Wong CH, Samuel M, Tan BK, Song C. Capsular contracture in subglandular breast augmentation with textured versus smooth breast implants: A systematic review. *Plast Reconstr Surg*. 2006;118(5):1224-1236. doi:10.1097/01.prs.0000237013.50283.d2.
5. Liu X, Zhou L, Pan F, Gao Y, Yuan X, Fan D. Comparison of the postoperative incidence rate of capsular contracture among different breast implants: A cumulative meta-analysis. *PLoS One*. 2015;10(2):1-18. doi:10.1371/journal.pone.0116071.
6. Poeppl N, Schreml S, Lichtenegger F, Lenich A, Eisenmann-Klein M, Prantl L. Does the surface structure of implants have an impact on the formation of a capsular contracture? *Aesthetic Plast Surg*. 2007;31(2):133-139. doi:10.1007/s00266-006-0091-y.
7. Headon H, Kasem A, Mokbel K. Capsular contracture after breast augmentation: An update for clinical practice. *Arch Plast Surg*. 2015;42(5):532-543. doi:10.5999/aps.2015.42.5.532.

8. Giot JP, Paek LS, Nizard N, et al. The double capsules in macro-textured breast implants. *Biomaterials*. 2015;67:65-72. doi:10.1016/j.biomaterials.2015.06.010.
9. Ramos-Gallardo G, Cuenca-Pardo J, Rodríguez-Olivares E, et al. Breast Implant and Anaplastic Large Cell Lymphoma Meta-Analysis. *J Investig Surg*. 2017;30(1):56-65. doi:10.1080/08941939.2016.1215576.
10. Loch-Wilkinson A, Beath KJ, Knight RJW, et al. Breast Implant-Associated Anaplastic Large Cell Lymphoma in Australia and New Zealand: High-Surface-Area Textured Implants Are Associated with Increased Risk. *Plast Reconstr Surg*. 2017;140(4):645-654. doi:10.1097/PRS.0000000000003654.
11. De Boer M, Van Der Sluis WB, De Boer JP, et al. Breast implant-associated anaplastic large-cell lymphoma in a transgender woman. *Aesthetic Surg J*. 2017;37(8):NP83-NP87. doi:10.1093/asj/sjx098.
12. De Boer M, Van Leeuwen FE, Hauptmann M, et al. Breast implants and the risk of anaplastic large-cell lymphoma in the breast. *JAMA Oncol*. 2018;4(3):335-341. doi:10.1001/jamaoncol.2017.4510.
13. Rupani A, Frame JD, Kamel D. Lymphomas associated with breast implants: A review of the literature. *Aesthetic Surg J*. 2015;35(5):533-544. doi:10.1093/asj/sjv016.
14. Bonnans C, Chou J, Werb Z. Remodelling the extracellular matrix in development and disease. *Nat Rev Mol Cell Biol*. 2014;15(12):786-801. doi:10.1038/nrm3904.
15. Steiert AE, Boyce M, Sorg H. Capsular contracture by silicone breast implants: Possible causes, biocompatibility, and prophylactic strategies. *Med Devices Evid Res*. 2013;6(1):211-218. doi:10.2147/MDER.S49522.
16. Issa R, Zhou X, Constandinou CM, et al. Spontaneous recovery from micronodular cirrhosis: Evidence for incomplete resolution associated with matrix cross-linking. *Gastroenterology*. 2004;126(7):1795-1808. doi:10.1053/j.gastro.2004.03.009.

17. Spear SL; Baker JL Jr. Classification of capsular contracture after prosthetic breast reconstruction. *Plast Reconstr Surg*. 1995;96:1119-1124.

18. Garabédian C, Delille R, Deltombe R, Anselme K, Atlan M, Bigerelle M. A multi-topographical-instrument analysis: the breast implant texture measurement. *Surf Topogr Metrol Prop*. 2017;5(2):025004. doi:10.1088/2051-672X/aa7290.

19. Brigaud I, Agniel R, Leroy-Dudal J, et al. Synergistic effects of BMP-2, BMP-6 or BMP-7 with human plasma fibronectin onto hydroxyapatite coatings: A comparative study. *Acta Biomater*. 2017;55:481-492. doi:10.1016/j.actbio.2017.04.013.

20. Brody GS, Deapen D, Taylor CR, et al. Anaplastic large cell lymphoma occurring in women with breast implants: Analysis of 173 cases. *Plast Reconstr Surg*. 2015;135(3):695-705. doi:10.1097/PRS.0000000000001033.

21. Barr S, Hill EW, Bayat A. Functional biocompatibility testing of silicone breast implants and a novel classification system based on surface roughness1. Barr, S., Hill, E. W. & Bayat, A. Functional biocompatibility testing of silicone breast implants and a novel classification sys. *J Mech Behav Biomed Mater*. 2017;75(May):75-81. doi:10.1016/j.jmbbm.2017.06.030.

22. Atlan M, Nuti G, Wang H, Decker S, Perry TA. Breast implant surface texture impacts host tissue response. *J Mech Behav Biomed Mater*. 2018;88:377-385. doi:10.1016/j.jmbbm.2018.08.035.

23. Jones P, Mempin M, Hu H, et al. The Functional Influence of Breast Implant Outer Shell Morphology on Bacterial Attachment and Growth. *Plast Reconstr Surg*. 2018;142(4):837-849. doi:10.1097/PRS.0000000000004801.

24. Ulrich D, Ulrich F, Pallua N, Eisenmann-Klein M. Effect of tissue inhibitors of metalloproteinases and matrix metalloproteinases on capsular formation around smooth and textured silicone gel implants. *Aesthetic Plast Surg*. 2009;33(4):555-562.

doi:10.1007/s00266-009-9335-y.

25. Kyle DJT, Harvey AG, Shih B, Tan KT, Chaudhry IH, Bayat A. Identification of molecular phenotypic descriptors of breast capsular contracture formation using informatics analysis of the whole genome transcriptome. *Wound Repair Regen*. 2013;21(5):762-769. doi:10.1111/wrr.12077.
26. Alaseem A, Alhazzani K, Dondapati P, Alobid S, Bishayee A, Rathinavelu A. Matrix Metalloproteinases: A challenging paradigm of cancer management. *Semin Cancer Biol*. 2017;(November):0-1. doi:10.1016/j.semcancer.2017.11.008.
27. Li A, Dubey S, Varney ML, Dave BJ, Singh RK. IL-8 Directly Enhanced Endothelial Cell Survival, Proliferation, and Matrix Metalloproteinases Production and Regulated Angiogenesis. *J Immunol*. 2003;170(3):3369-3376. doi:10.4049/jimmunol.170.6.3369.
28. Rundhaug JE. Matrix metalloproteinases and angiogenesis. *J Cell Mol Med*. 2005;9(2):267-285. doi:10.1111/j.1582-4934.2005.tb00355.x.
29. Baggiolini M, Loetscher P, Moser B. Interleukin-8 and the chemokine family. *Int J Immunopharmacol*. 1995;17(2):103-108. doi:10.1016/0192-0561(94)00088-6.
30. Fouque-Aubert A, Chapurlat R. Influence of RANKL inhibition on immune system in the treatment of bone diseases. *Jt Bone Spine*. 2008;75(1):5-10. doi:10.1016/j.jbspin.2007.05.004.
31. Taishin Akiyama, Yusuke Shimo JQ. RANKL signaling controls the develop- ment of regulatory T cells RANKL signaling regulates lymph node development RANKL signaling regulates the microen- vironment of the thymus. 2009;23(1):258-262.
32. Rao S, Cronin SJF, Sigl V, Penninger JM. RANKL and RANK: From Mammalian Physiology to Cancer Treatment. *Trends Cell Biol*. 2017;28(3):213-223. doi:10.1016/j.tcb.2017.11.001.
33. Chong SJ, Deva AK. Understanding the Etiology and Prevention of Capsular

Contracture. *Clin Plast Surg*. 2015;42(4):427-436. doi:10.1016/j.cps.2015.06.007.

34. Brown T, Harvie F, Stewart S. A Different Perspective on Breast Implant Surface Texturization and Anaplastic Large Cell Lymphoma (ALCL). *Aesthetic Surg J*. 2019;39(1):56-63. doi:10.1093/asj/sjy091.

35. Mempin M, Hu H, Chowdhury D, Deva A, Vickery K. The A, B and C's of Silicone Breast Implants: Anaplastic Large Cell Lymphoma, Biofilm and Capsular Contracture. *Materials (Basel)*. 2018;11(12):2393. doi:10.3390/ma11122393.